

pubs.acs.org/journal/ascecg

# Hydrothermal Liquefaction of Acid Whey: Effect of Feedstock **Properties and Process Conditions on Energy and Nutrient Recovery**

Hanifrahmawan Sudibyo, Kui Wang,\* and Jefferson William Tester\*



Cite This: ACS Sustainable Chem. Eng. 2021, 9, 11403-11415



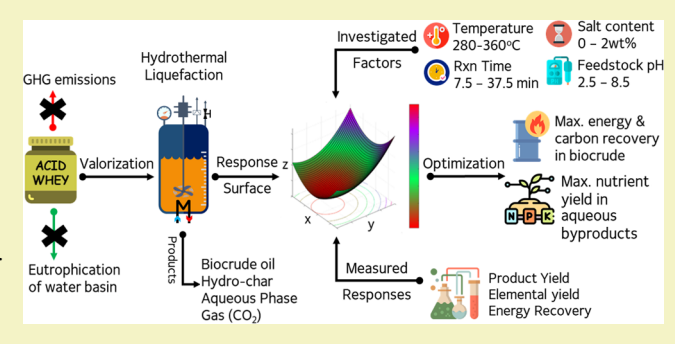
**ACCESS** I

III Metrics & More

Article Recommendations

Supporting Information

ABSTRACT: Improper management of dairy wastewater (acid whey) leads to water basin eutrophication and greenhouse gas emissions. We evaluated hydrothermal liquefaction as a means to sustainably manage and valorize acid whey wastes by converting them into biocrude oil and recovering nutrients in aqueous-phase byproducts. In a set of well-defined experiments, we studied the effects of reaction temperatures (280-360 °C), reaction times (7.5-37.5 min), feedstock pH values (2.5-8.5), and feedstock salt contents (0-2 wt %) on the energy recovered and the yields of products and elements. Response surface analysis showed that an alkaline feedstock pH (8.5) and a short reaction time (7.5 min) combined with a specific optimal reaction temperature for certain



salt content in the feedstock were required to maximize biocrude energy recovery and nutrient recovery for a range of feedstock compositions. In general, 280–290 °C was optimal for salt contents ≤1.675 wt % and 360 °C for salt contents 1.675–2 wt %. Carbon and nitrogen were mostly distributed between biocrude and aqueous-phase products, added with distribution to the gas phase at higher temperatures. Partitioning of inorganics, for example, calcium and phosphorus, into aqueous-phase and solid hydrochar products depended on reaction conditions. This study provides new information for controlling target product composition as well as specifying desirable operating conditions for practical systems.

KEYWORDS: dairy waste, acid whey, hydrothermal liquefaction, energy recovery, nutrient recovery, response surface methodology, product formation pathway, element distribution pathway

# **■** INTRODUCTION

The increasing trend toward consumption of nutrient-dense dairy products such as soft-cheese and protein-rich Greek-style yogurt as a signature of a healthy lifestyle has contributed to the mass production of new waste management challenges. Acid whey is a liquid byproduct of soft-cheese and concentrated Greek-style yogurt production that is mostly composed of water (94-96%), lactose (3-4%), protein (0.5-1%), and salt (0.5-2.6%). 1-6 A detailed physicochemical composition of typical acid whey is given in Table S1. According to annual production data on Greek yogurt, sour cream, and soft cheese (cottage, ricotta, and cream) released by the USDA ERS in 2019, an estimated 10 million metric tons of acid whey is produced in the United States each year. Unlike sweet whey, which has gained market as a raw material for nutraceuticals and other food additives, acid whey is still underutilized due to its low protein content, more acidic taste, and high salinity. These properties limit its use as a fertilizer to low value-added applications such as land application, where rapid infiltration of whey into the soil can cause excessive nutrient runoff to the water bodies. The presence of excessive nutrients leads to eutrophication or nutrient enrichment-primarily from nitrogen and phosphorus—of water sources that triggers algae bloom and hypoxia.8 In addition, acid whey is categorized as an easily biodegradable and high organic loading wastewater, indicated by the biological oxygen demand/chemical oxygen demand (COD) ratio >0.5 and the COD of 30,000-50,000 mg/L, potentially causing degradation in water quality as well as the emission of greenhouse gases.9

The development of innovative thermochemical methods such as hydrothermal liquefaction (HTL) to recover carbon, energy, and nutrients can mitigate environmental problems related to the mismanagement of wet biomass wastes like acid whey. HTL takes advantage of the unique properties of liquid water at near-supercritical conditions where its ion product  $(K_w)$ increases at pressures up to 10-20 MPa from  $10^{-\bar{1}4}$  at 25 °C to  $10^{-11}$  at 300 °C and then decreases to  $10^{-13}$  at 360 °C. These conditions result in higher ionic reactivity as both acid and base catalysts and result in a lower water dielectric constant, which

Received: May 19, 2021 Revised: August 3, 2021 Published: August 15, 2021





increases solubility for less polar compounds. <sup>10,11</sup> Other important benefits of the HTL conversion process include its ability to sterilize wastewater, recover energy by concentrating carbon into biocrude oil, and recycle nutrients by precipitation into the hydro-char or by extraction into the aqueous phase.

HTL chemical reaction pathways and rates greatly depend on process conditions and feedstock properties, including temperature, reaction time, pH, the concentration of solids, and inorganics (ash) content. Optimizing these factors is a major step toward producing desirable outcomes of the treatment such as high energy recovery or high carbon yield in biocrude oil with ultralow content of heteroatoms and high nutrient yield in the aqueous phase for recycling. The literature on optimizing process conditions for energy and nutrient recovery using HTL suggests a wide range of methods for different feedstocks. <sup>12–25</sup>

Previous studies have suggested 280–320 °C and 15–60 min as the optimum range for reaction temperature and reaction time, respectively, to produce high bio-oil yield with high carbon content from microalgae, a mixture of model compounds, and animal manure digestate, although higher temperatures have also been reported. 12,13,18,19,26 Both alkaline and acidic conditions have been reported to improve the carbon recovery in biocrude oil by suppressing hydro-char formation and catalyzing oil production. A solid concentration 10–35 wt % in the feedstock is also favored to obtain high energy recovery. 10,13,19,23,27 However, a high inorganic (ash) content in the feedstock has been reported to be detrimental for biomass conversion to bio-oil. 28

The optimal process conditions for HTL of biomass waste become more complex when nutrient recovery is coupled with energy recovery. In a study of element distributions from HTL of Spirulina, Miscanthus, and primary sludge, Madsen and Glasius<sup>24</sup> concluded that high-protein feedstocks like Spirulina need to be treated at either a low temperature and a short reaction time (250 °C and 5 min) or a high temperature and a long reaction time (350 °C and 31 min) to obtain low nitrogen content in the biocrude oil, while lignocellulosic biomass like Miscanthus and primary sludge favor a combination of high temperature (350 °C) and short reaction time (5 min). A study by Fan et al.<sup>18</sup> reported an increase in nitrogen recovery in biocrude oil when the temperature for HTL of lactose/maltose with lysine was raised from 250 to 350 °C. To recover nitrogen in the aqueous phase as ammonia nitrogen (NH<sub>3</sub>-N) for nutrient recycling, Yang et al. 25 reported that adding acid (HCl) and base (Na<sub>2</sub>CO<sub>3</sub>) catalysts yielded high concentrations of NH<sub>3</sub>-N between 5000 and 6000 mg/L for the HTL of Tetraselmis sp. at 350 °C. Similarly, Song et al. 12 reported that the NH<sub>3</sub>-N yield in the aqueous phase of the HTL of Cyanophyta increases from 250 to 350 °C.

In terms of phosphorus recovery, hydrothermal treatment at mild operating conditions using an acidic medium has been found to successfully transform most phosphorus into the inorganic form via a thermal-oxidative mechanism, leading to phosphorus migrating into the aqueous phase. <sup>14,15</sup> A preference for reclaiming phosphorus in the aqueous phase rather than in the hydro-char has been explained by Ghanim and co-workers. They identified the phosphorus species in the solid residue from the HTL of phosphorus-rich poultry litter as inorganic apatite phosphate, which is not bioavailable to plants if the hydro-char is used as a soil fertilizer. <sup>16</sup> An additional extraction step using a mineral acid such as  $H_2SO_4$  has been suggested by Ovsyannikova et al. <sup>17</sup> to effectively extract phosphorus from

hydro-char and convert it into a slow-release fertilizer, in this case, struvite.

Coupling energy and nutrient recovery for acid whey treatment requires an understanding of the combined effects of feedstock properties and process conditions to determine the intersection of the corresponding optimal conditions. The lack of a detailed mechanistic understanding of these combined factors motivated our study. Our approach focused on (1) characterizing the effect of feedstock properties and process conditions on the formation of HTL products, the yields of elements in the products, and the energy recovery in biocrude through the use of a feedstock with well-defined composition and (2) optimizing the HTL process conditions to maximize energy and nutrient recovery from different feedstock compositions. To achieve these objectives, a synthetic acid whey (SAW) was employed for our experiments.

In addition, we utilized central composite design (CCD) for specifying the experimental design. CCD is a type of response surface methodology (RSM), which can be applied with the desirability function approach<sup>29</sup> for multicriteria optimization. Further details about RSM, CCD, and desirability function approach can be found in the literature. <sup>29–31</sup> Four factors were selected as independent variables: HTL reaction temperature, reaction time, feedstock pH, and salt content. Feedstock pH and salt content can fluctuate depending on the milk source and type of milk-derivative products. To control the pH and the salt content, SAW solutions were prepared with specific compositions and used as feedstocks in our experiments. Water content and organics composition were considered uniform for acid whey because its range of moisture content is narrow (94–96 wt %), lactose concentration is 3–4 wt % and constitutes 60–75% of the dry matter, and nitrogen in acid whey majorly exists as amino acids with the amino-acid-to-lactose weight ratio between 1:7 and 1:6. 4,5,11 Multiple responses were measured to develop several response models using RSM. The optimizations at the specified feedstock compositions were performed to generate five response surfaces relevant for energy and nutrient recovery: carbon yield (maximized), energy recovery (maximized), and nitrogen yield (minimized) in biocrude, phosphorus yield (maximized), and ammonia nitrogen yield (maximized) in the aqueous phase. The optimization results were validated through additional experiments.

## MATERIALS AND METHODS

**Materials.** SAW was prepared by mixing anhydrous lactose (Medisca), L-glutamic acid (BioBasic), KH<sub>2</sub>PO<sub>4</sub> (Macron Fine Chemicals), Ca-lactate (Santa Cruz Biotechnology), KCl (EMD Chemicals), NaOH (Sigma Aldrich), and citric acid (Merck) with 200 mL of water (18.2 MΩ·cm). L-glutamic acid was chosen as a model amino acid to supply organic nitrogen because glutamic acid is the largest component of whey protein. <sup>32,33</sup> The composition of SAW for the experiment is given in Table S3. Acetone, dichloromethane, and ethyl acetate in ACS grade (Fisher Chemical) were used for biocrude oil extractions. Anhydrous MgSO<sub>4</sub> (Santa Cruz Biotechnology) was used for drying the biocrude solvent mixtures before solvent evaporation. Analytical reagents for colorimetric measurement were purchased from Hanna Instruments.

**Experimental Design.** Thirty-one experiments were conducted consisting of 16 factorial points, 8 axial points, and 1 six-time-replicated center point (see Table S2 for a complete CCD matrix). The range of values for each factor is shown in Table 1. The range for reaction temperature and reaction time was based on optimal energy and nutrient recovery values reported in the literature. <sup>14,16,24,34,35</sup> The pH range (2.5–8.5) was selected based on the reported pH of dairy

Table 1. Factor Levels for CCD of HTL of SAW

variables	factor levels				
	-2	-1	0	1	2
$X_1$ : temperature (°C)	280	300	320	340	360
$X_2$ : reaction time (min)	7.5	15	22.5	30	37.5
$X_3$ : initial feedstock pH	2.5	4	5.5	7	8.5
$X_4$ : salt content (wt %)	0	0.5	1	1.5	2

industry effluents.<sup>3,4</sup> The salt content range was chosen based on the reported salt and ash contents for different types of whey.<sup>2,5,6</sup>

Data generated from the CCD-based experiments were fitted into eq 1 using factor levels to obtain coded coefficients by maintaining the hierarchical form

$$Y = \alpha_0 + \sum_{i=1}^{n} \alpha_i X_i + \sum_{i=1}^{n} \alpha_{ii} X_i^2 + \sum_{i=1}^{n-1} \sum_{j=i+1}^{n} \alpha_{ij} X_i X_j$$
 (1)

where Y is the response function-dependent variable,  $\alpha_0$  is the intercept,  $X_i$  is an independent variable in a set of n=4 variables defined in Table 1, and  $\alpha_v$ ,  $\alpha_{iv}$  and  $\alpha_{ij}$  serve as fitted coefficients of linear, quadratic, and interaction terms, respectively. The model fitting was statistically evaluated according to the p-value of model terms <0.05,  $R^2$ ,  $R^2$  (pred.), and lack-of-fit p-value >0.05. The regression model fitting, the response optimization using the desirability function approach, and the making of contour plots were performed in Minitab 19.2.0 and MATLAB 2020b

Hydrothermal Liquefaction. HTL experiments were conducted in a 500 mL Parr 4575 SS316 reactor equipped with a Parr 4878 controller to adjust reaction temperature and stirring speed (130 rpm). The reactor was loaded with varying amounts of feedstock according to the experimental design. The sealed reactor was purged and prepressurized with N<sub>2</sub> gas to 300 psi (2.07 MPa) and heated to the reaction temperature. The heating times for room temperature to reach the reaction temperatures of 280, 300, 320, 340, and 360 °C were around 45, 50, 60, 70, and 80 min, respectively (Figure S1). Statistical analysis of the effect of heating time on all response variables showed a p-value >0.05 (Tables S4 and S5), which indicates that the heating time effect is not significant for all responses. The reaction time was arbitrarily started when the targeted temperature was reached. At the end of the experiment, the reactor was cooled to room temperature by flowing water through the internal cooling coil and depressurized before the reactor was opened to collect the product. The product separation followed the same procedures as explained by Wang et al.<sup>3</sup> The recovered products include three biocrude extraction fractions, hydro-char, and the liquid byproduct after extraction (aqueous phase). The three biocrude fractions are dichloromethane-extracted (DL) and ethyl acetate-extracted (EL) water-soluble biocrudes, and dichloromethane-extracted solid-bound biocrude (DW).

**Product Analysis.** The yields of biocrude or hydro-char were calculated using eq 2.

$$Yield_{i} = \frac{m_{i}}{m_{feedstock}} \times 100\%$$
(2)

where Yield is the mass yield of product, i is biocrude or hydro-char, m is the product mass (g), and  $m_{\rm feedstock}$  is the dry mass of feedstock (g). The total biocrude yield is the sum of the yield of the three biocrude fractions.

Carbon, hydrogen, and nitrogen contents in biocrude and hydrochar were measured in triplicate using a CE-440 Elemental Analyzer (Exeter Analytical). The carbon yields in biocrude and hydro-char were calculated using eq 3.

$$X_{\text{yield-i}} = \frac{(\%X_{i}) \times m_{i}}{X_{\text{feedstock}}} \times 100\%$$
(3)

where  $X_{\text{yield}}$  and %X are the carbon yield and the carbon content (wt %) in the product, respectively, i is biocrude or hydro-char, m is the product mass (g), and  $X_{\text{feedstock}}$  (g) is total carbon in the feedstock. Likewise,

nitrogen yield in biocrude and hydro-char can also be calculated using eq 3 where  $X_{\rm yield}$  and %X are nitrogen yield and nitrogen content, respectively, and  $X_{\rm feedstock}$  is total nitrogen in the feedstock. The total yield of carbon or nitrogen in the biocrude  $(C_{\rm yield-Oil})$  or  $N_{\rm yield-Oil})$  was taken as the sum of carbon or nitrogen yield of the three biocrude fractions. The H/C and O/C atomic ratios for the biocrude fraction were calculated based on the yield and elemental composition of each fraction.

The yields of carbon and nitrogen in the aqueous phase ( $C_{yield-AP}$  and  $N_{vield-AP}$ ) were calculated using eqs 4 and 5.

$$C_{\text{yield-AP}} = \frac{\text{TOC}_{\text{LP}} \times V_{\text{LP}}}{\text{total C in feedstock}} \times 100\% - C_{\text{yield-WSO}}$$
 (4)

$$N_{\text{yield-AP}} = \frac{TN_{\text{LP}} \times V_{\text{LP}}}{\text{total N in feedstock}} \times 100\% - N_{\text{yield-WSO}}$$
 (5)

where  $TOC_{\rm LP}$  and  $TN_{\rm LP}$  are total organic carbon and total nitrogen concentration (g/L) in the liquid phase, respectively, measured using an automated Shimadzu TOC-L and TNM-L analyzer module,  $V_{\rm LP}$  is the volume of liquid phase (L), and  $C_{\rm yield\text{-}WSO}$  and  $N_{\rm yield\text{-}WSO}$  are carbon and nitrogen yield in water-soluble biocrude (DL and EL fractions), respectively.

Carbon and nitrogen lost to the gas phase ( $C_{yield-Gas}$  and  $N_{yield-Gas}$ ) were estimated by the difference using the known amount of carbon and nitrogen in the biocrude, hydro-char, and aqueous phase (eqs 6 and 7). Afterward, the gas yield was estimated based on carbon yield in the gas phase using eq 8 by assuming that the gas was mostly composed of  $CO_2$ . This assumption was confirmed in Tables S6 and S7. The yield of the aqueous phase product was calculated using eq 9.

$$C_{\text{yield-Gas}} = 100\% - C_{\text{yield-Oil}} - C_{\text{yield-HC}} - C_{\text{yield-AP}}$$
 (6)

$$N_{\text{yield-Gas}} = 100\% - N_{\text{yield-Oil}} - N_{\text{yield-HC}} - N_{\text{yield-AP}}$$
 (7)

$$Yield_{Gas} = \frac{44}{12} \times \frac{C_{yield-Gas} \times (C \text{ in feedstock})}{m_{feedstock}} \times 100\%$$
(8)

$$Yield_{AP} = 100\% - Yield_{Biocrude} - Yield_{HC} - Yield_{Gas}$$
 (9)

The yield of each inorganic nutrient (X = P, K, or Ca) in the hydrochar ( $X_{yield-HC}$ ) was calculated using eq 10.

$$X_{\text{yield-HC}} = \frac{m_{\text{HC}} \times \% \text{Ash}_{\text{HC}} \times \% X_{\text{ash}}}{\text{total X in feedstock}} \times 100\%$$
 (10)

where  $m_{\rm HC}$  is the hydro-char mass (g), %Ash<sub>HC</sub> is the hydro-char ash content (wt %) determined gravimetrically following the ASTM E1755-01 standard method, <sup>38</sup> and %X<sub>Ash</sub> is the elemental concentration in hydro-char ash (wt %) measured using energy-dispersive X-ray spectroscopy (Oxford Instruments). The ash was also analyzed for the mineral composition using an X-ray powder diffractometer (Bruker D8 Advance ECO) and quantitated in MDI Jade 7.8.2 following the whole pattern fitting and Rietveld refinement method.

The yield of each inorganic nutrient ( $X = NH_3-N$ , P, K, or Ca) in the aqueous phase ( $X_{yield-AP}$ ) was calculated using eq 11.

$$X_{\text{yield-AP}} = \frac{[X]_{\text{AP}} \times V_{\text{AP}}}{\text{total X in feedstock}} \times 100\%$$
 (11)

where  $V_{\rm AP}$  represents aqueous phase volume (L) and [X]\_{\rm AP} (g/L) represents the nutrient concentration in the aqueous phase measured using a HI83399 photometer (Hanna Instruments). The measurement for phosphorus was carried out using the amino acid method (APHA 4500-P), that for NH<sub>3</sub>-N was done using the Nessler method (ASTM D1426-15), that for potassium was done using the turbidimetric tetraphenylborate method, and that for calcium was done using the oxalate method. The yield of organic nitrogen in the aqueous phase (Org-N<sub>yield-AP</sub>) was calculated by the difference between N<sub>yield-AP</sub> and NH<sub>3</sub>-N<sub>yield-AP</sub>. To measure the inorganics content in the biocrudes, thermogravimetric analysis was performed by heating biocrude samples at 20 °C/min to 950 °C (TA Instruments QA500).

Table 2. Regression Models for Product Yield (%) and pH Change of the Liquid Phase (pH<sub>liq</sub> change)

response variables	coded equations	$R^2$	R <sup>2</sup> (pred.)	lack-of-fit <i>p</i> - value	center point
biocrude yield	$Y = 23.174 - 0.063T - 0.615t + 1.037pH - 1.463Salt - 0.594T^{2}$	85.89%	75.69%	0.165	$22.90 \pm 0.47\%$
hydro-char yield	$Y = 16.135 - 0.72T + 0.302t - 2.745pH - 0.7pH^{2}$	87.47%	71.51%	0.184	$16.66 \pm 0.29\%$
aqueous phase yield	$Y = 49.342 - 1.741T - 1.861t + 2.937pH - 0.226Salt - 2.903Salt^2$	82.29%	66.21%	0.448	$49.54 \pm 2.21\%$
gas yield	$Y = 12.368 + 2.524T + 2.174t + 1.807Salt + 2.881Salt^2$	76.83%	62.20%	0.290	$10.89 \pm 2.36\%$
$pH_{liq}$ change	$Y = -1.5366 + 0.2513T - 0.0963t \ 1.2029pH + 0.0038Salt + 0.0893T^2 - 0.1219(pH)(Salt)$	99.35%	98.72%	0.561	$-1.56 \pm 0.06$

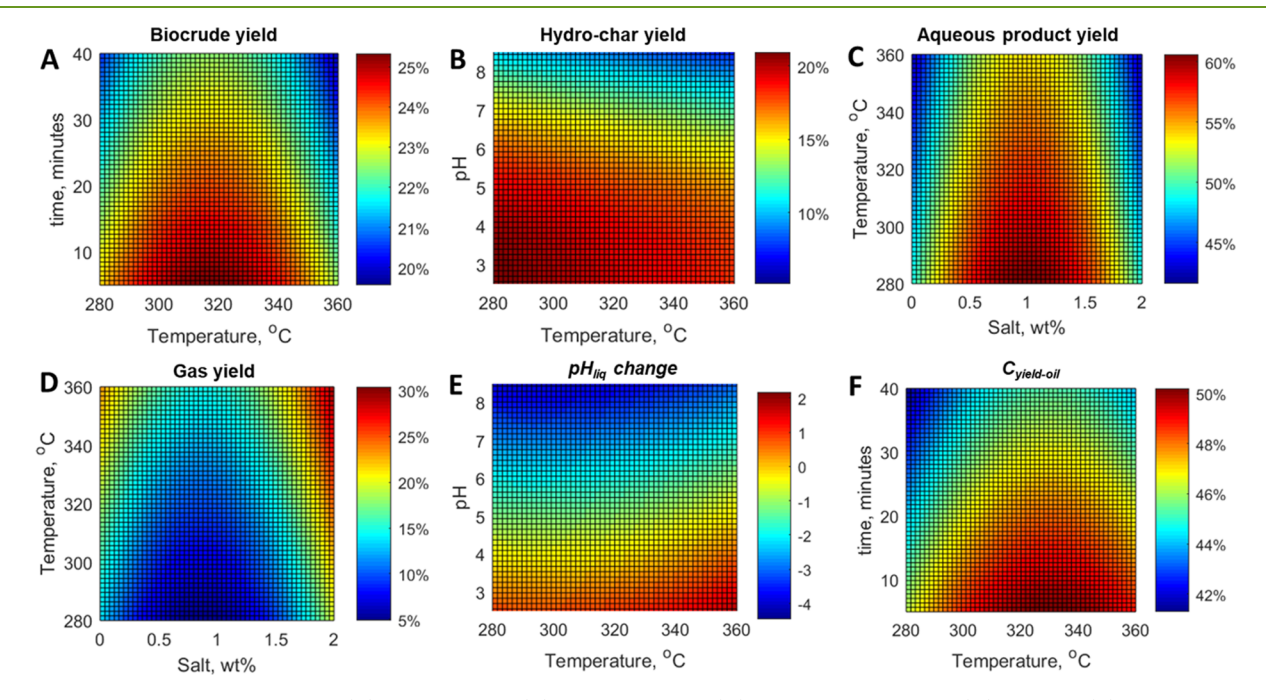


Figure 1. Representative contour plots for (A) biocrude yield, (B) hydro-char yield, (C) aqueous product yield, (D) gas yield, (E) pH changes of liquid phase after reaction (pH $_{liq}$  change), and (F) carbon yield in biocrude ( $C_{vield-oil}$ ).

Higher heating values (HHV, MJ/kg) of the dry feedstock (HHV $_{\rm feedstock}$ ) and biocrude (HHV $_{\rm Oil}$ ) were calculated using eq 12 with elemental compositions as percentages. <sup>44</sup> The energy recovery in biocrude (ER $_{\rm oil}$ ) was calculated using eq 13 where ER $_{\rm oil}$  was taken as the sum of energy recovery of the three biocrude extraction fractions.

$$HHV = 0.349C + 1.1783H - 0.1034O - 0.015N - 0.021Ash$$
 (12)

$$ER_{oil} = \frac{m_{Oil} \times HHV_{Oil}}{m_{feedstock} \times HHV_{feedstock}} \times 100\%$$
(13)

# ■ RESULTS AND DISCUSSION

In general, this section is divided into two parts. The first part, from the Product Yields to the Distribution of Inorganics subsection, begins by laying out the effects of process variables on the formation of products, biocrude energy recovery, and elemental distributions between the product phases, followed by establishing the product and element distribution pathways. In these subsections, the data from measurements of different response variables are presented as contour plots. The contour plots were made by varying two statistically significant variables (x-axis and y-axis) and holding all other variables constant at factor level zero (see Table 1 for the natural value of factor level zero). A complete set of contour plots for each response can be found in Figures S2–S27. The reproducible error of the response variable is reflected by the average and the standard

deviation of six replicated center-point experiments. The discussion employs regression equations in coded units (i.e., independent variables standardized on the factor level scale) to determine which variable is more and/or the most important by comparing the coefficient value of each term. Only statistically significant terms are included in the equations. Throughout the text, statistically significant variables or terms are those having a p-value <0.05. Data of the p-value of each significant variable/ term for each response and regression equations in uncoded units (unstandardized independent variable) are presented in Tables S8-S16. The second part, the multicriteria optimization subsection, presents the optimum process conditions to maximize the energy and nutrient recovery from feedstocks with different compositions. Validation of the optimization results and the discussion of the dominant distribution pathway from the corresponding optimum process conditions are also presented in this subsection.

**Product Yields.** *Biocrude.* Measured total biocrude yields in this study ranged from 18.97 to 26.53%, in agreement with previous studies.  $^{18,28,37,45,46}$  The DW fraction contained the highest yield, followed by the DL and EL fractions for all experimental conditions. The quadratic model for biocrude yield had a good fit without overfitting the data ( $R^2$ (pred.) is close to  $R^2$ ), as indicated by statistical measures in Table 2. The effects of reaction temperature and time, feedstock pH, and salt content on biocrude yields were statistically significant (p <

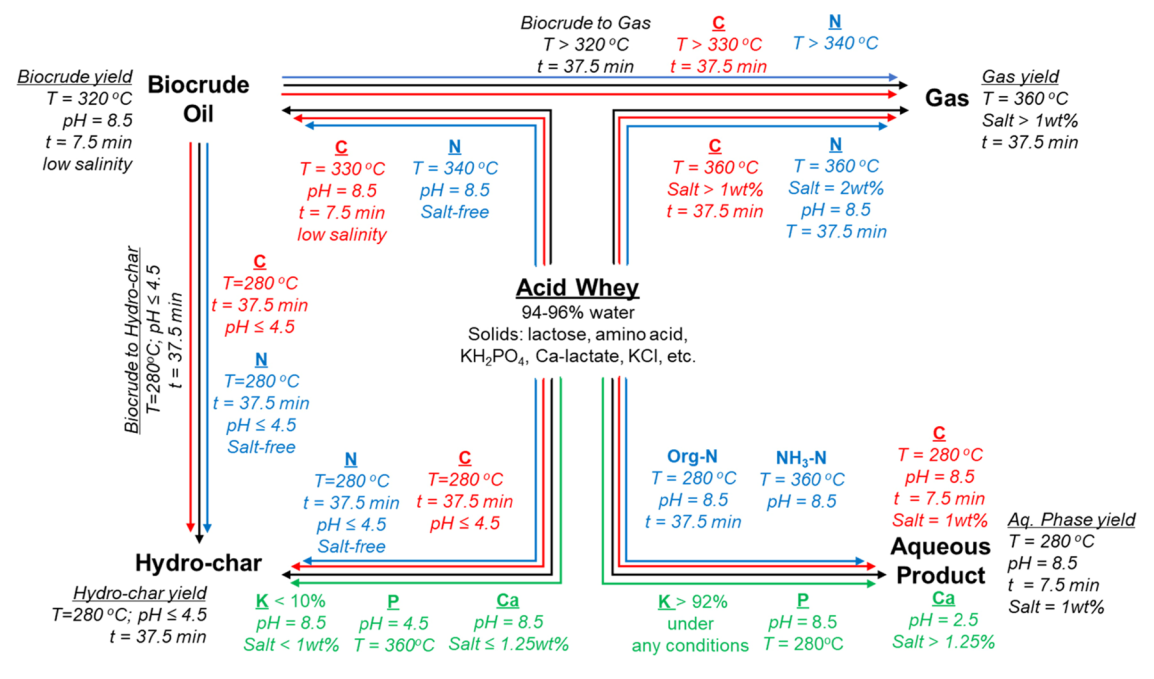


**Figure 2.** Suggested product (black arrows) and element (red—C, blue—N, and green—P, K, and Ca) distribution pathways with favorable conditions to increase the product or elemental yield are attached to every arrow. The optimum condition of factors that do not have maxima or minima is defined by either the lowest (factor level—2) or the highest value (factor level 2).

0.05). Increasing salt content lowered biocrude yield (the linear coefficient for salt content is negative), which is consistent with earlier work by Liu and co-workers.<sup>28</sup> They reported that inorganic salt inhibits the transformation of biomass to biocrude by covering the surface of organic species that consequently limits the heat and mass transfer during HTL, leading to a lower biocrude production. The linear coefficient for feedstock pH was positive, indicating that alkaline feedstock promotes biocrude production. Based on the linear coefficient for reaction time, which is negative in the biocrude yield model and positive in the hydro-char and gas yield model, increasing reaction time beyond 7.5 min was observed to linearly lower biocrude yield and increase hydro-char and gas yield (Table 2). This indicates that at prolonged reaction times over 7.5 min, chemical species in the biocrude are subjected to depolymerization (cracking) and hydro-char formation as competing reactions. Temperature gave a negative effect correlated with a quadratic dependence, showing a peak in biocrude yield around 320 °C, after which biocrude yield decreased due to partial decomposition, as shown in Figure 1A. The decomposition was associated with the conversion into gas because the increasing temperature increased the gas yield (the linear coefficient for temperature in the gas yield model is positive).

*Hydro-Char*. The hydro-char yield ranged between 7.26 and 18.98%, similar to that reported in the literature.  $^{13,18,19,47}$  The quadratic model provided a good fit and a capability of predicting accurately using a new observation according to the model performances in Table 2. The most pronounced effect was given by feedstock pH, as shown by the largest negative linear coefficient for feedstock pH (Table 2). The hydro-char yield stabilized around 20% at feedstock pH  $\leq$  4.5 (Figure 1B) due to the small quadratic effect of pH and was largely reduced at feedstock pH > 4.5. As the feedstock pH increased past 4.5, the role of the acidic degradation pathway for carbohydrates became less important. The acidic pathway has been reported to produce furanic compounds and precursors for hydro-char formation

through polymerization and aromatization in the liquid phase. A less significant linear effect was observed from reaction temperature and time, as indicated by their smaller negative and positive linear coefficients, respectively. An increase in temperature lowers the hydro-char yield because higher temperatures enhance the conversion of the feedstock into biocrude and gas. The rising temperature may also enhance the temperature-dependent Maillard reaction between carbohydrates and amino acids, which inhibits hydro-char formation by blocking the conversion of carbohydrates into furans (hydro-char precursors). Als, An increase in hydro-char yield over extended reaction time indicates that hydro-char formation is a time-dependent process.

Aqueous Phase. The yield of aqueous phase products ranged between 35.17 and 56.81%. The quadratic model fitted the aqueous phase yield data well, and the intercept was larger than for the other product yield models (Table 2). According to the coefficient of the significant term in the aqueous phase yield's model (Table 2), feedstock pH gave a positive linear effect, while reaction temperature and reaction time gave a linear negative effect. The positive linear effect of feedstock pH on the aqueous product yield was associated with the production of acids because the final pH of the liquid phase after HTL treatment was largely reduced when the feedstock pH was higher (see  $pH_{\text{liq}}$ change in Table 2 and Figure 1E). On the other hand, increasing temperature (Figure 1C) and lengthened reaction time led to a lower yield of aqueous products due to the conversion of some organics into gas. This result corresponded with the positive linear effect/coefficient of reaction temperature and reaction time in the gas yield model (Table 2). A quadratic dependence of aqueous product yield on salt content was observed. Increasing salt content up to 1 wt % increased aqueous product yield, but past 1 wt %, the aqueous product yield decreased (Figure 1C). This decrease was related to the conversion of the aqueous products into gas because the gas yield continuously increased with salt content >1 wt % (Figure 1D). Previous

Table 3. Regression Models for Carbon Yield (%) and Biocrude Energy Recovery (ER<sub>oil</sub>, %)

response variables	coded equations	$R^2$	$R^2$ (pred.)	lack-of-fit p-value	center point
$C_{yield-Oil}$	$Y = 44.158 + 1.105T - 1.061t + 3.624 \text{ pH} - 1.572Salt - 0.625T^2$	87.06%	74.68%	0.161	$43.86 \pm 1.10\%$
$C_{\text{yield-HC}}$	$Y = 23.53 - 1.036T + 0.403t - 5.757pH - 2.213Salt - 0.832pH^2$	95.74%	89.21%	0.206	$23.92 \pm 1.05\%$
$C_{ ext{yield-AP}}$	$Y = 23.32 - 18.47T - 1.104t + 3.048pH - 2.588Salt - 1.076Salt^2$	83.62%	73.87%	0.137	$24.35 \pm 1.06\%$
$C_{yield ext{-}Gas}$	$Y = 9.266 + 1.403T + 1.887t + 1.739Salt + 1.638Salt^{2}$	69.74%	58.32%	0.102	$7.88 \pm 1.71\%$
$ER_{Oil}$	Y = 42.895 + 1.462T - 0.968t + 3.847pH - 1.118Salt	84.19%	76.20%	0.148	$42.56 \pm 1.16\%$

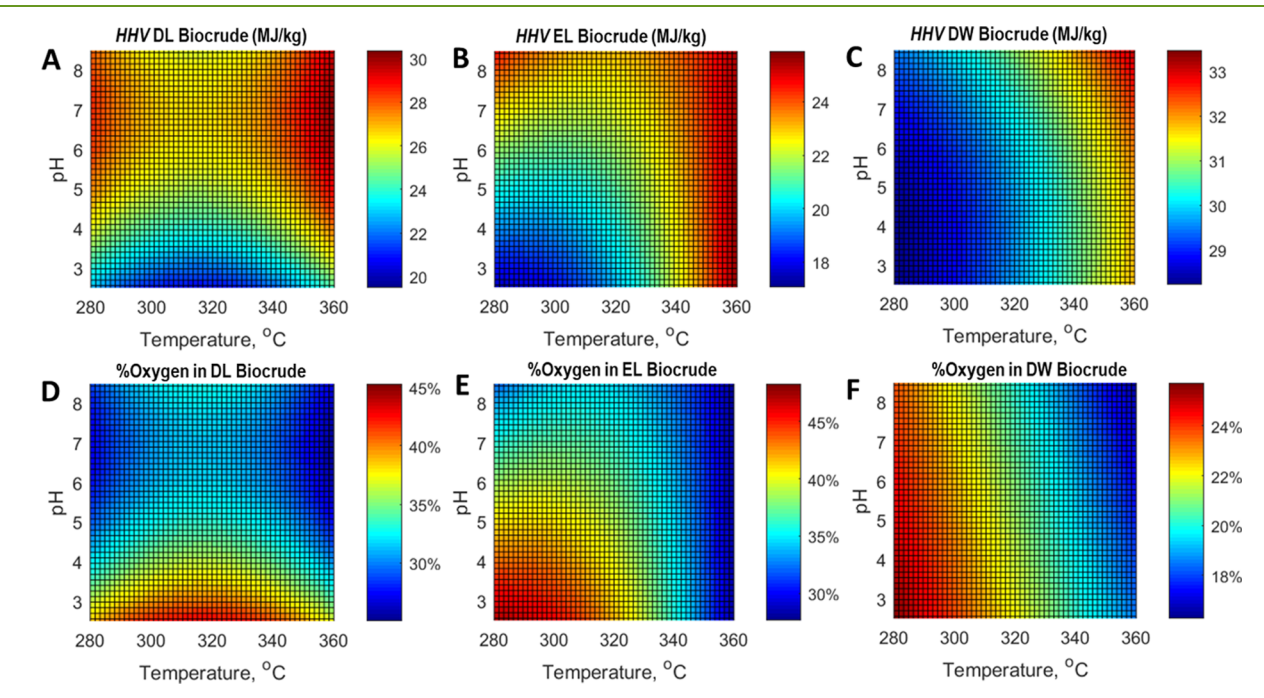


Figure 3. Representative contour plots for higher heating value (HHV) and oxygen content in DL (A and D), EL (B and E), and DW (C and F) biocrudes.

studies have reported that alkali metals like calcium and potassium, which exist in acid whey salt, can catalyze gasification of aqueous organics like short-chain carboxylic acids to form  ${\rm CO}_2$ . On the other hand, although the trend of gas yield was negative from salt content 0 to 1 wt % (Figure 1D), this did not mean that salt content <1 wt % also led to producing more gas. The negative trend of gas yield was caused by the relatively constant amount of gas produced over the increasing amount of dry feedstock at a higher salt content (see Figure S6).

A product formation pathway for the HTL of SAW is proposed based on the abovementioned results (Figure 2). The conversions of the feedstock (lactose, glutamic acid, etc.) into biocrude oil and aqueous-phase products are assumed to occur first based on the effect of reaction time at a constant temperature. The relatively similar optimal conditions for the maximum yield of biocrude and aqueous products indicate that the formation of biocrude and aqueous products can occur concurrently.<sup>24</sup> The hydro-char formation can come from two ways: repolymerization of biocrude fragments and repolymerization of furanic compounds produced from the decomposition of feedstock. The feedstock decomposition also produces organics, particularly acids that are readily converted into gas phase products when the reaction severity is very high (higher reaction temperatures and longer reaction times). Similarly, biocrude cracking may also contribute to the gas production at high-severity process.

Carbon Yield and Biocrude Energy Recovery. In this study, carbon yield in biocrude was generally higher than carbon

yield in the other products. Biocrude carbon yield (C<sub>yield-Oil</sub>) varied from 36.25 to 54.26%, while carbon yield in hydro-char  $(C_{\text{yield-HC}})$  and the aqueous phase  $(C_{\text{yield-AP}})$  was between 11.20 and 33.15%, and 12.56and 30.99%, respectively. Carbon yield in the gas phase ( $C_{\text{yield-Gas}}$ ) was the lowest (2.62–19.23%). The effects of process parameters on carbon yield in every product were almost identical to those for product yields, according to Tables 2 and 3. The differences were that the linear coefficient for reaction temperature was positive in the  $C_{\text{yield-Oil}}$  model and salt content gave a negative linear effect on C<sub>vield-HC</sub>. The former caused a slightly higher optimum temperature than that for biocrude yield to recover up to 54% of carbon in the biocrude at 330 °C (Figure 1F). The latter resulted in  $C_{yield-HC}$  as low as 4% when combined with alkaline feedstock pH and high reaction temperature (Figure S9). All contour plots for carbon yield in each product phase are presented in Figures S7-S10. Because most independent variables had similar effects on product yield and carbon yield, it can be concluded that moderate temperature, short reaction time, high feedstock pH, and low salt content are also favored to gain as much carbon as possible in the biocrude. This finding also leads to an understanding that the carbon distribution pathway resembles the product formation pathway, as demonstrated by Figure 2.

The HHV of biocrude ranged between 20 and 32 MJ/kg, in agreement with values reported in the literature.  $^{53,54}$  A broad range of energy recovery values was found for biocrude (ER<sub>Oil</sub>) (36–53.70%), and the linear model was significant with a good fit (Table 3). The effects of all factors were strongly linear for

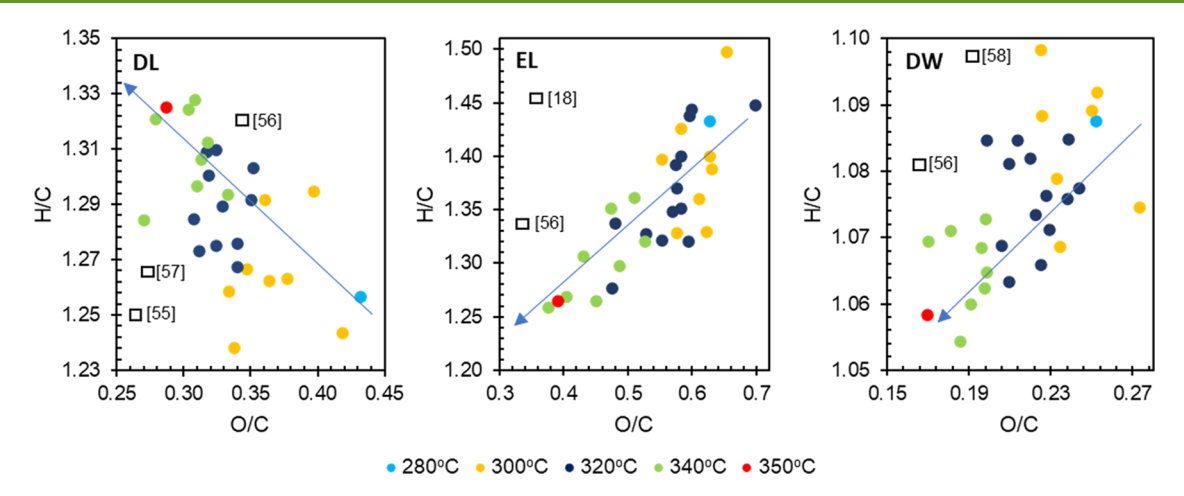


**Figure 4.** Van Krevelen diagram for DL, EL, and DW biocrudes, including some results from previous studies on HTL of protein-containing biomass. <sup>18,55–58</sup> The diagonal arrow from the bottom right to top left indicates decarboxylation and from top right to bottom left indicates dehydration.

Table 4. Regression Models for Nitrogen Yield (%)

response variables	coded equations	$R^2$	R <sup>2</sup> (pred.)	lack-of-fit <i>p</i> -value	center point
$N_{yield-Oil}$	$Y = 46.291 + 2.841T + 0.86t + 4.697pH + 1.508Salt - 1.578T^2 - 2.722(pH)(Salt)$	78.96%	62.83%	0.176	$46.66 \pm 2.41\%$
$N_{yield-HC}$	$Y = 33.69 - 2.566T + 0.597t - 10.186pH - 2.886Salt - 1.452pH^2$	95.88%	89.80%	0.498	$33.76 \pm 1.39\%$
$ m Org$ - $ m N_{yield-AP}$	Y = 7.808 - 3.087T + 0.595t + 1.874pH - 2.375(T)(t) - 1.202(T) (pH)	76.26%	61.39%	0.322	$7.51 \pm 1.69\%$
$\mathrm{NH_{3^-}} \ \mathrm{N_{yield\text{-}AP}}$	Y = 19.402 + 3.291T + 0.256t + 3.683pH	82.52%	76.79%	0.270	$15.13 \pm 0.55\%$
$N_{yield ext{-}Gas}$	$Y = 2.444 + 0.2862T - 0.0492t + 1.3323pH + 0.278Salt + 0.2447T^2 + 0.2361t^2 + 0.7442pH^2 + 0.1415Salt^2 + 0.1701(T)(pH) + 0.3354 (pH)(Salt)$	97.69%	91.57%	0.570	$15.13 \pm 0.55\%$

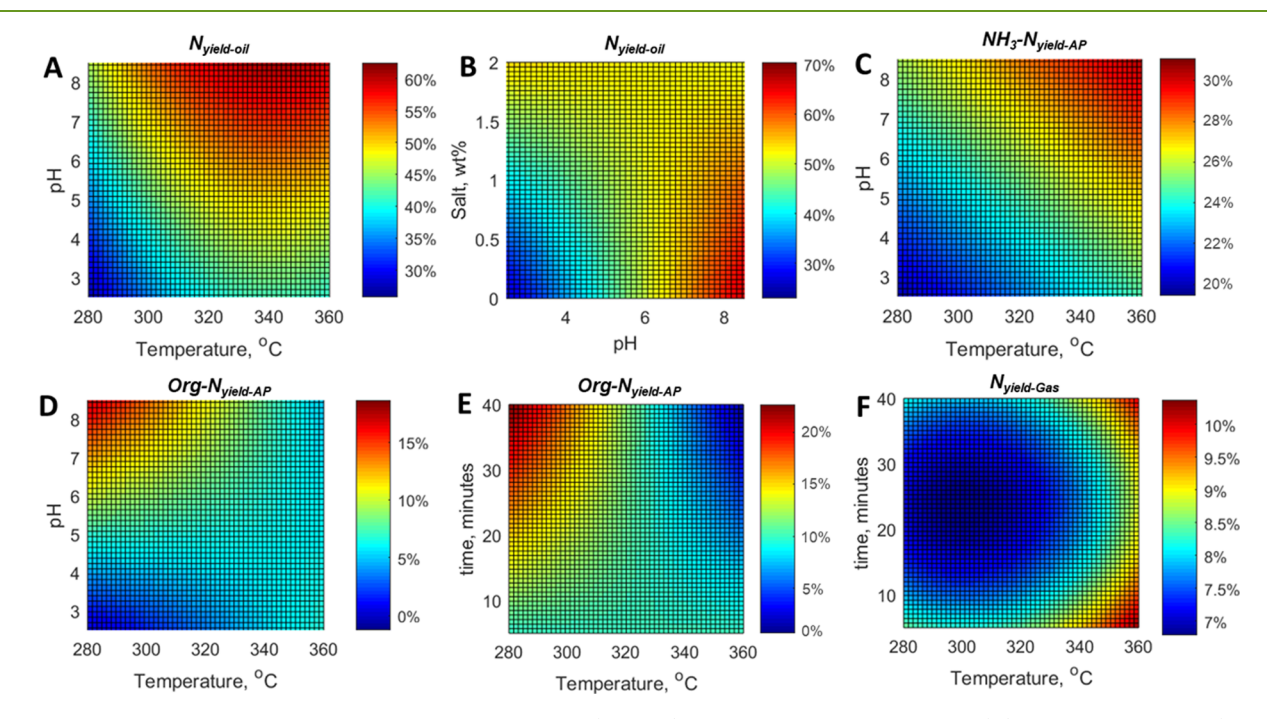


Figure 5. Representative contour plots for nitrogen yield in biocrude (A and B), in the aqueous phase as  $NH_3$ -N (C) and organic nitrogen (D and E), and in the gas phase (F).

 $ER_{Oil}$ , similar to those for the biocrude yield and  $C_{yield-Oil}$ , except for its temperature dependence. Previously, a quadratic effect of temperature was identified for the biocrude yield and  $C_{yield-Oil}$ , yielding maxima at 320 and 330 °C, respectively. Nonetheless, the effect of temperature on  $ER_{Oil}$  was linearly positive, which

means that higher energy recovery can still be obtained, although  $C_{\rm yield-Oil}$  decreases at temperatures higher than 330 °C. From eq 13,  $ER_{\rm Oil}$  was determined by the HHV of the biocrude, HHV of the feedstock, and biocrude yield. With HHV of the feedstock remaining constant, the biocrude mass yield was

observed to decrease at temperatures higher than 320  $^{\circ}$ C. However, ER<sub>Oil</sub> increased linearly at higher temperatures caused by a larger improvement in HHV of the biocrude product (Figure 3) to sufficiently compensate for the decrease in biocrude mass yield. The significant increase of biocrude HHV at higher temperatures was due to a substantial decrease in oxygen content as illustrated in Figure 3. The removal of oxygen from the biocrude may occur via decarboxylation and dehydration. According to the Van Krevelen diagram shown in Figure 4, increasing temperature generally led to expelling oxygen via decarboxylation for DL biocrude and dehydration for EL and DW biocrudes.

Nitrogen Yield. Biocrude. The nitrogen yield in biocrude (N<sub>vield-oil</sub>) varied between 27.85 and 53.19%, similar to those reported in previous studies on HTL of protein-containing biomass at 250–350 °C. <sup>18,59,60</sup> The quadratic model performed satisfactorily (Table 4) without overfitting the noise in the N<sub>vield-oil</sub> data. Feedstock pH was the most significant factor with the largest positive linear coefficient. Rising feedstock pH increased the N<sub>vield-oil</sub> and could lead to fixing up to 60% of nitrogen from the feedstock into the biocrude product (Figure 5A). The N<sub>vield-oil</sub> dependence on feedstock pH can be explained by considering the pH change of the liquid phase after reaction (pH<sub>liq</sub> change). According to Table 2 and Figure 1E, pH<sub>liq</sub> change showed a larger decrease when the feedstock pH measured before the reaction was higher or more alkaline, implying that more acids were produced from alkaline feedstocks. Acids produced from the alkaline feedstock not only can lower the pH, but they can also serve as reactive participants in the Maillard reaction to produce heterocyclic nitrogen compounds, such as pyrrole, pyridine, and pyrazine derivatives that are less polar and soluble in the biocrude phase. 18,46 For instance, pyruvic aldehyde is an acid produced from the alkaline degradation of lactose, and Peterson et al. 61 have reported that pyruvic aldehyde is a more reactive reactant in the Maillard reaction than the reducing sugars (monosaccharides, lactose, and maltose) because it is noncyclic, has two carbonyls, and has smaller molecular size. The fixation of nitrogen from the alkaline feedstock into the biocrude via Maillard reaction started to be inhibited when the salt content increased. The interaction between feedstock pH and salt content lowered the N<sub>vield-oil</sub>, as indicated by the negative coefficient for feedstock pH-salt interaction term (Table 4). Figure 5B illustrates the negative trend of N<sub>vield-oil</sub> when the salinity in alkaline feedstock increases. However, a positive trend of  $N_{\text{yield-oil}}$  was observed when the increasing salinity occurred in the acidic feedstock (pH < 6.5). The positive trend of N<sub>yield-oil</sub> was caused by the catalytic effect of the increasing phosphate salt concentration on the Maillard reaction. In an acidic medium (pH 2.5-6.5), phosphate salt is ionized into metal cations and dihydrogen phosphate anions. A study by Guan and co-workers<sup>62</sup> reported that dihydric phosphate radical anions could function as a hydrogen donor and acceptor to catalyze the formation of glycosylamines and the intermediates in the Maillard reaction.

Another significant factor for  $N_{yield-oil}$  was temperature, which gave a quadratic effect.  $N_{yield-oil}$  increased from 280 to 340 °C (Figure 5A) before slowly dropping at higher temperatures due to the decomposition of biocrude carbons that began at 330 °C, fairly close to 340 °C. Nitrogen heteroatoms in chemical compounds are mostly present in the form of C–N bonds so that the thermal-oxidative partial decomposition of carbon from biocrude can involve the destruction of C–N bonds, which consequently releases nitrogen. Nitrogen release from biocrude

to the aqueous phase as  $NH_3$ -N or the gas phase was assumed to be prominent because the ammonia nitrogen yield in the aqueous phase ( $NH_3$ - $N_{yield-AP}$ ) and the nitrogen yield in gas ( $N_{yield-gas}$ ) increased at temperatures higher than 340 °C, as shown by Figure 5C,F. Meanwhile, the effect of reaction time on the  $N_{yield-oil}$  was positive but less pronounced than the other factors, as indicated by the smallest positive linear coefficient (Table 4).

*Hydro-Char.* The yield of nitrogen in hydro-char ( $N_{yield-HC}$ ) was between 11.99 and 52.85%. The quadratic model fitted the data adequately (Table 4). The value of  $R^2$  (pred.) is very close to  $R^2$ , indicating that the model can predict well enough for future observations. The effects of temperature, feedstock pH, and reaction time on the nitrogen yield in hydro-char ( $N_{yield-HC}$ ) were similar to those for hydro-char yield (Tables 2 and 4). This resemblance indicates that  $N_{yield-HC}$  is highly correlated with hydro-char yield. Interestingly, salt content had a negative linear effect on  $N_{yield-HC}$ , whereas its effect was insignificant for the hydro-char yield (Table 2). This negative effect was due to lower nitrogen content in hydro-char produced from feedstock with higher salt content (see Figure S26).

Aqueous Phase. Nitrogen yield in the aqueous phase is classified into organic nitrogen (Org-N<sub>yield-AP</sub>) and ammonia nitrogen (NH<sub>3</sub>-N<sub>yield-AP</sub>) with a yield of 1.39–19.35% and 7.78– 30.26%, respectively. The quadratic model provided a good fit for  $Org-N_{vield-AP}$ , and the linear model performed very well for  $NH_3$ - $N_{yield-AP}$  (Table 4). The effect of feedstock pH and reaction temperature were statistically significant for NH3-Nyield-AP and Org-N<sub>yield-AP</sub>. The NH<sub>3</sub>-N<sub>yield-AP</sub> and Org-N<sub>yield-AP</sub> increased with feedstock pH, as shown by Figure 5C,D, respectively. As discussed earlier, alkaline feedstock promotes massive acid production. Such acids may catalyze the hydrolysis of amino acids to generate NH3-N and amines through the deamination and decarboxylation pathways, respectively.63 However, the positive effect of feedstock pH on the Org-N<sub>yield-AP</sub> gradually decreased with the increasing reaction temperature and reached a plateau at a temperature higher than 340 °C (see Figure 5D). A negative interaction was also seen between reaction temperature and reaction time for Org-N<sub>yield-AP</sub> in Table 4. Figure 5Edemonstrates the negative trend of  $Org-N_{yield-AP}$  when the increasing reaction temperature is accompanied by a reaction time longer than 15 min. In contrast, the effect of temperature on NH<sub>3</sub>-N<sub>vield-AP</sub> was linearly positive, which suggests that deamination is enhanced at higher temperatures.

Gas Phase. The nitrogen yield in the gas phase ( $N_{yield-gas}$ ) ranged between 2.38 and 8%. The quadratic model fitted the data satisfactorily with all linear and quadratic terms, and two interaction terms, temperature-pH and pH-salt content, in the model were statistically significant (Table 4). Global minima are shown by all contour plots (see Figures 5F and S20). Overall, global minima for  $N_{yield-gas}$  were located at 300–325 °C, 24 min, feedstock pH of 4.25, and salt content of 0–1.1 wt %. These process conditions can be chosen to minimize nitrogen transfer to the gas.

A nitrogen distribution pathway into HTL products is suggested in Figure 2. The pathway is similar to the product formation pathway, added with the classification of nitrogen in the aqueous phase into ammonia and organic fractions. From the abovementioned results, it can be concluded that low temperature (280 °C), short reaction time (7.5 min), and acidic feedstock (pH 2.5) should be employed to keep the nitrogen distribution into the biocrude as low as possible. At these conditions,  $N_{\rm yield\mbox{-}oil}$  can be reduced to 20–25% (Figure 5A),

Table 5. Model Results for Mineral Nutrient Yield (%)

response variables	coded equations		$R^2$ (pred.)	lack-of-fit <i>p</i> -value	center point
Ca <sub>yield-AP</sub>	$Y = 36.9 - 20.75 \text{pH} - 0.0028 Salt + 5.58 \text{pH}^2 + 6.31 (\text{pH})(Salt)$	88.64%	80.99%	0.199	$35.01 \pm 3.13\%$
$Ca_{yield ext{-HC}}$	$Y = 59.53 + 20.55pH + 4.95Salt - 4.13pH^2 - 6.28(pH)(Salt)$	87.87%	77.61%	0.179	$64.49 \pm 3.07\%$
$P_{yield-AP}$	$Y = 12.01 - 4.224T + 6.641pH + 5.61pH^2$	69.45%	55.30%	0.107	$13.79 \pm 0.43\%$
$P_{\text{yield-HC}}$	$Y = 84.89 + 4.11T - 5.37pH - 4.47pH^{2}$	77.78%	63.24%	0.487	$82.41 \pm 0.84\%$
$K_{yield-AP}$	$Y = 93.48 - 1.092 \text{pH} - 0.243 \text{Salt} + 0.458 \text{pH}^2 + 0.642 \text{Salt}^2 + 1.068 (\text{pH})(\text{Salt})$	78.45%	66.29%	0.386	$93.36 \pm 0.76\%$
$K_{yield ext{-}HC}$	$Y = 5.03 + 1.024 \text{pH} - 0.146 \text{Salt} - 0.264 \text{pH}^2 - 0.151 \text{Salt}^2 - 0.927 (\text{pH})(\text{Salt})$	76.11%	62.54%	0.209	$4.34 \pm 0.18\%$

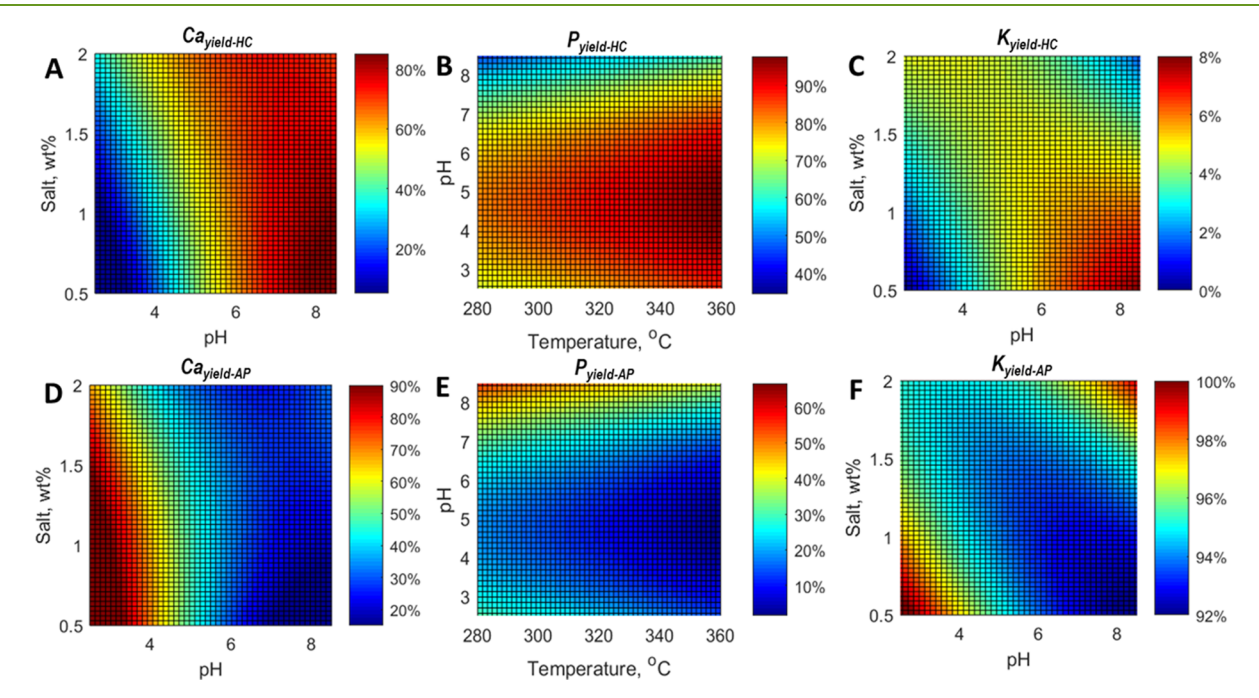


Figure 6. Contour plots for the yield of calcium, phosphorus, and potassium in hydro-char (A, B, and C, respectively) and the yield of calcium, phosphorus, and potassium in the aqueous phase (D, E, and F, respectively).

with around 55% of the nitrogen in the feedstock is distributed into the hydro-char (Figure S21). With  $N_{yield-oil}$  of 20–25%, the nitrogen content in the biocrudes is 0.4–1.4% (Figures S23–S25), still greater than the maximum allowable nitrogen content for direct integration into petroleum refining industries that is 0.25%. The remaining 20–25% of feedstock nitrogen is distributed into the aqueous (15–20% as NH<sub>3</sub>-N and 0–5% as organic nitrogen) and the gas phase (around 5%; see Figure S20).

Distribution of Inorganics. Extraction into the aqueous phase and immobilization into the solid hydro-char phase were two major processes that controlled the fate of inorganics during the HTL of SAW. In this study, the distribution of inorganics to the biocrude was not considered for two reasons: (1) The total yield of inorganics in hydro-char and the aqueous phase was always close to 100% and (2) thermogravimetric analysis results of biocrudes produced from the feedstock with the highest salt content (2 wt %) and the feedstock that produced the least hydro-char (feedstock pH of 8.5) showed no measurable residues (Figures S28 and S29). Measured inorganic element yields were reasonably correlated using the quadratic model without indication of overfitting as reflected by the statistical measures in Table 5.

The yields of calcium in hydro-char (Ca<sub>yield-HC</sub>) and the aqueous phase (Ca<sub>yield-AP</sub>) were 14.67–81.49% and 16.18–84.93%, respectively. According to Table 5, the significant terms affecting calcium partitioning were feedstock pH, salt content,

and the interaction between these two factors. The trend of Ca<sub>yield-HC</sub> with the rising salt content was positive at feedstock pH < 6, and its trend was slightly negative at feedstock pH > 6.5, while in general, Ca<sub>yield-HC</sub> increased with feedstock pH (Figure 6A), and vice versa for the trend of Ca<sub>yield-AP</sub> (Figure 6D). The positive trend of Ca<sub>yield-HC</sub> against feedstock pH was due to the precipitation of CaCO<sub>3</sub> and Ca-apatite in the hydro-char (Figure S27). Alkaline pH is favored by calcium to precipitate as carbonate and apatite minerals in the hydro-char. In addition, the increasing trend of Ca<sub>yield-HC</sub> with feedstock pH also indicated a higher calcium content in the hydro-char because hydro-char yield decreased with feedstock pH.

The yields of phosphorus in hydro-char ( $P_{yield-HC}$ ) and the aqueous phase ( $P_{yield-AP}$ ) were 45.75–92.02% and 6.47–55.17%, respectively (Figure 6B,E).  $P_{yield-HC}$  and  $P_{yield-AP}$  were controlled by the reaction temperature and feedstock pH, as described in Table 5. The linear effect of temperature on  $P_{yield-HC}$  and  $P_{yield-AP}$  showed positive and negative trends, respectively, which means that higher reaction temperatures enhance the precipitation/fixation of phosphorus in hydro-char, similar to what has been reported in the literature. A statistically more significant impact was given by feedstock pH, which shows a quadratic effect with maxima for  $P_{yield-HC}$  and minima for  $P_{yield-AP}$  located at pH 4.5 as demonstrated in Figure 6B,E. The decrease in  $P_{yield-HC}$  at feedstock pH greater than 4.5 was associated with the decreasing hydro-char yield (Figure 1B). Meanwhile, the decrease in  $P_{yield-HC}$  at pH less than 4.5 was due to the higher

solubility of phosphorus in a highly acidic medium. While this result indicates that both acidic and alkaline feedstocks are capable of lowering phosphorus immobilization in hydro-char via different mechanisms, the observed minima in  $P_{yield-AP}$  at pH 4.5 suggests that a highly acidic feedstock (pH < 2.5) would be needed to extract the same amount of phosphorus as the process that uses slightly alkaline feedstock.

Among all mineral nutrients, only potassium was almost completely extracted into the aqueous phase. The yield of potassium in the aqueous phase ( $K_{\rm yield-AP}$ ) was 91.70–97.75% and that in the hydro-char ( $K_{\rm yield-HC}$ ) was 2.55–8.83%, excluding the experiment that employed zero salt content. In the model for  $K_{\rm yield-AP}$  and  $K_{\rm yield-HC}$  presented in Table 5, the quadratic terms of feedstock pH and salt content were significant, similar to the interaction term between the two factors. This leads to a ridge of maximum  $K_{\rm yield-HC}$  for feedstock pH of 8.5 and salt content of 0.7 wt % (Figure 6C). The contour plot for  $K_{\rm yield-AP}$  in Figure 6E shows that a trough-like shape with a maximum  $K_{\rm yield-AP}$  was due to both the acidic feedstock with low salt content and the alkaline feedstock with high salt content. Figure 2 summarizes the optimum conditions to maximize the yield of nutrients in every product phase.

**Multicriteria Optimization.** Experimental designs focused on determining the optimum temperature, reaction time, and feedstock pH in response to the varying salt content in the feedstock. Although feedstock pH may fluctuate depending on the milk feedstock, type of milk-derivative products, and selected production process, the feedstock pH can be more easily adjusted by adding acid or base. The optimization results in the form of desirability plots and a summary table are presented in Figure S30 and Table S17.

Over the range of feedstock salt contents studied from 0 to 2 wt %, the optimum reaction time and feedstock pH remained consistent at 7.5 and 8.5 min, respectively. The optimum reaction temperature was also consistent at 280  $^{\circ}$ C for a feedstock salt content of 0–1 wt %. It slightly increased from 280 to 290  $^{\circ}$ C for a feedstock salt content of 1–1.675 wt % and reached a plateau at 360  $^{\circ}$ C when the salt content was >1.675 wt % (Figure 7).

According to the desirability plots presented in Figure S30, the increasing salt content must be countered with increasing temperature because salt content negatively affected the

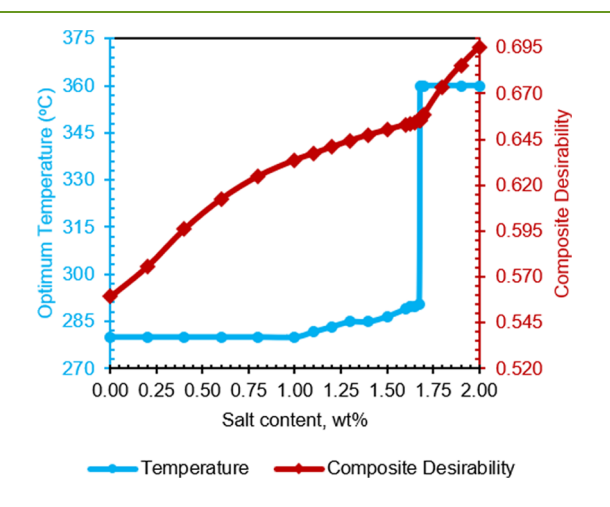


**Figure 7.** Profiles of optimum reaction temperature and composite desirability at various feedstock salt contents and at constant feedstock pH of 8.5 and reaction time of 7.5 min.

individual desirability of  $ER_{oil}$  and  $C_{yield\text{-}oil}$ , which in turn decreased the composite desirability. The temperature was the only factor that could be altered to improve the desirability of ERoil and Cyield-oil because the effect of feedstock pH on the composite desirability was positive, which implies that pH of 8.5 should be implemented at any salt content. Likewise, employing a short reaction time (7.5 min) was also favored because the long reaction time lowered the composite desirability. Increasing reaction temperature lowers the dielectric constant of water and consequently lowers the solubility of inorganic salts and leads to precipitating more salts. 65 With less amount of dissolved inorganic salt due to precipitation, the inhibiting effects of salts on the thermochemical conversion of the organic species into biocrude oil were reduced, leading to improvement in biocrude yield and carbon/energy recovery in biocrude. Although increasing temperature reduced P<sub>vield-AP</sub> due to precipitation and fixation in hydro-char, the reduction was still acceptable because the individual desirability of Pvield-AP was only slightly lowered and still very close to the composite desirability (Figure S30).

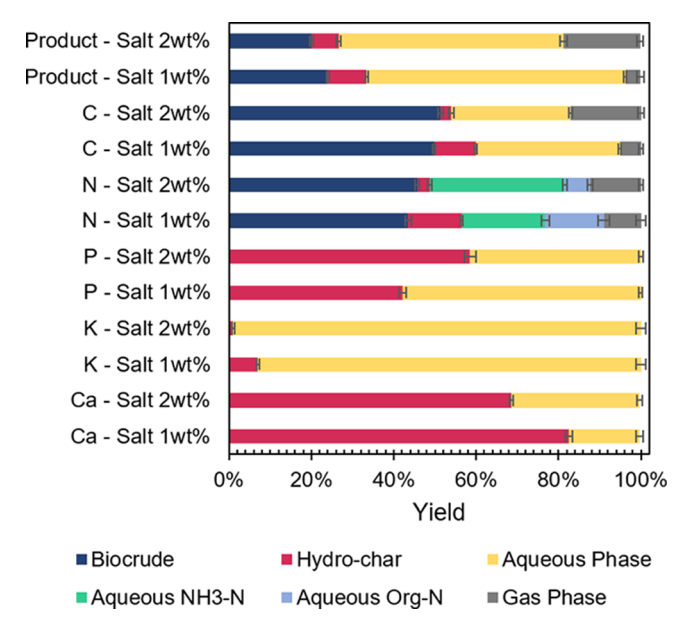
Additional experiments employing the optimum conditions for salt content 1 and 2 wt % were performed in triplicate to validate the optimization results. The comparison between the predicted and experimental values of each response presented in Table 6 verified the validity and reproducibility of the

Table 6. Validation of Optimization Results for Salt Content 1 and 2 wt %

optimized responses	salt 1 wt %		salt 2 wt %		
	pred.	exp.	pred.	exp.	
$C_{yield-Oil}$	48.82%	$49.81 \pm 0.32\%$	50.10%	$51.36 \pm 0.08\%$	
$N_{yield-Oil}$	41.97%	$43.48 \pm 0.70\%$	45.47%	$45.74 \pm 0.20\%$	
ER <sub>Oil</sub>	49.60%	$48.87 \pm 0.89\%$	53.21%	$53.03 \pm 0.44\%$	
$\mathrm{NH_{3}\text{-}N_{yield\text{-}AP}}$	19.67%	$20.32 \pm 0.92\%$	32.84%	$32.75 \pm 0.15\%$	
$P_{yield-AP}$	56.18%	$56.79 \pm 0.22\%$	39.28%	$40.78 \pm 0.31\%$	

optimization results. The final distribution of the product and elemental yield based on the additional experiments is illustrated in Figure 8.

Figure 8 illustrates the dominance of the formation pathway of biocrude and aqueous product when SAW with salinity ≤1 wt % and feedstock pH of 8.5 was treated at 280 °C and 7.5 min, as shown by the total yield of biocrude and aqueous product that reached 86.8%. However, higher temperature treatment (>280 °C) for SAW with salinity >1 wt % boosted the gas production with a gas yield of up to 18.6% at 360 °C, 7.5 min, feedstock pH of 8.5, and salt content 2 wt %. This drastic increase in gas production was caused by the higher reaction temperatures initiating partial biocrude and aqueous organics decomposition into gas products. In addition, the higher salt content promoted gasification of aqueous organics similar to what was observed earlier at salt contents >1 wt % (see Figure 1D). Meanwhile, the role of the hydro-char formation pathway was found to be minimal, as its yield was always lower than 10% and decreased with temperature. Thus, increasing temperature to 360 °C to overcome the adverse effect of salt content on the energy/ carbon recovery resulted in three major product formation pathways: aqueous product, biocrude, and gas. A similar pattern to the product formation pathway was also observed for the carbon and nitrogen distribution pathway. For potassium and calcium, the major distribution pathways were extracted into the



**Figure 8.** Yields of products and elements in HTL products based on validation experiments for feedstock with salt content 1 wt % (280 °C, pH 8.5, 7.5 min) and 2 wt % (360 °C, pH 8.5, 7.5 min).

aqueous phase ( $K_{\rm yield-AP} > 90\%$ ) and precipitated and fixated in the hydro-char, respectively, under any process conditions. Meanwhile, the distribution of phosphorus, which was initially controlled by partitioning into the aqueous phase at lower temperatures, shifted toward being dominated by precipitation/fixation in the hydro-char at 360 °C.

# **■ CONCLUSIONS AND RECOMMENDATIONS**

Our study on HTL of SAW provided new understandings of how feedstock properties and process conditions affected HTL product formation, elemental distribution, and energy recovery. Response surface analysis revealed the significance of an alkaline pH (8.5) for the feedstock, a short reaction time (7.5 min), low reaction temperatures (280-290 °C) for feedstock with salt contents  $\leq 1.675$  wt %, and high reaction temperature (360 °C) for feedstock with salt contents 1.675-2 wt % in maximizing carbon/energy recovery in biocrude oil and nutrient recovery in the aqueous-phase byproducts. Specific roles of the alkaline feedstock pH were suppressing hydro-char formation, maximizing biocrude oil production, concentrating carbon in the biocrude phase, retaining phosphorus in the aqueous phase, and producing acids that may catalyze the formation of aqueousphase NH<sub>3</sub>-N via deamination of amino acid. Short reaction time minimized partial decomposition of biocrude oil into gas or repolymerization into hydro-char. Low reaction temperatures lessened nitrogen fixation into the biocrude and phosphorus precipitation in solid hydro-char. Meanwhile, applying high reaction temperature for processing high-salinity feedstock reduced the inhibiting effects of salts on biocrude oil production by lowering the amount of dissolved inorganic salt in the reaction medium (near-supercritical water) via precipitation. Solubility of salt in near-supercritical water decreases with temperature due to the lower dielectric constant of water. These results demonstrate that recovering energy and nutrients using HTL to valorize wet biomass waste, such as acid whey, can be effectively done by specifying desirable operating conditions for a range of feedstock compositions to control target product composition.

Nonetheless, the produced biocrudes still contained 1.2-1.8% nitrogen and 17-37% oxygen, which makes direct integration into petroleum refinery operations technically infeasible at present. Future research is required to identify conditions where employing heterogeneous catalysts during HTL would facilitate the production of biocrudes with ultralow content of heteroatoms, that is, N < 0.25% and O < 2.7%. Additionally, the nutrients recovered in the aqueous phase still require further processing to transform them into a usable form. Methods to recover NH<sub>3</sub>-N and phosphorus from the aqueous phase are worth investigating, such as conversion to solid struvite or liquid fertilizer concentrates and/or removal of ammonia by steam stripping and biodegradation. In addition, in future studies, nutrients recycled using separation methods such as membrane filtration should be considered to facilitate the integration of nutrient co-product recovery with HTL processing.

#### ASSOCIATED CONTENT

# Supporting Information

The Supporting Information is available free of charge at https://pubs.acs.org/doi/10.1021/acssuschemeng.1c03358.

Experimental design and feedstock compositions; statistics of the heating time effect; estimated gas phase compositions; *p*-value of significant terms in the regression equations; regression equations of all response variables (in uncoded unit); contour plots of all response variables; thermogravimetric curves of selected biocrude samples; and desirability plots and summary table for multicriteria optimization (PDF)

## AUTHOR INFORMATION

## **Corresponding Authors**

Kui Wang — School of Chemical and Biomolecular Engineering and Energy Systems Institute, Cornell University, Ithaca, New York 14853, United States; oocid.org/0000-0003-4743-5442; Phone: 315-244-9009; Email: kw587@cornell.edu

Jefferson William Tester — School of Chemical and Biomolecular Engineering and Energy Systems Institute, Cornell University, Ithaca, New York 14853, United States; Phone: 617-877-4696; Email: jwt54@cornell.edu

#### Author

Hanifrahmawan Sudibyo — School of Chemical and Biomolecular Engineering and Energy Systems Institute, Cornell University, Ithaca, New York 14853, United States; Chemical Engineering Department, Universitas Gadjah Mada, Yogyakarta 55281, Indonesia; © orcid.org/0000-0003-1905-129X

Complete contact information is available at: https://pubs.acs.org/10.1021/acssuschemeng.1c03358

#### **Author Contributions**

The manuscript was written through the contributions of all authors. H.S.: conceptualization, methodology, investigation, formal analysis, data curation, and writing—original draft. J.W.T. and K.W.: conceptualization, methodology, writing—review and editing, and supervision.

#### Notes

The authors declare no competing financial interest.

## ACKNOWLEDGMENTS

The authors thank for the financial support provided by the Cornell Energy Systems Institute, the Atkinson Center for a Sustainable Future, the Graduate School at Cornell, the U.S. Department of Energy (DOE) as a part of the DOE's process intensification research in their RAPID program, and the USDA grant 2019-69012-29905 for carrying out the study. The first author (H.S.) also thanks the Fulbright-DIKTI Foundation for support as a doctoral candidate in chemical engineering at Cornell University. This work also made use of the Cornell Center for Materials Research Facilities (NSF MRSEC DMR-1719875).

## REFERENCES

- (1) Farkye, N.; Quark, Y. Quark-like Products, and Concentrated Yogurts. Cheese: Chem., Phys. Microbiol. (4th Ed.) 2017, 1, 1103–1110.
- (2) Blaschek, K. M.; Wendorff, W. L.; Rankin, S. A. Survey of Salty and Sweet Whey Composition from Various Cheese Plants in Wisconsin. *J. Dairy Sci.* **2007**, *90*, 2029–2034.
- (3) Carvalho, F.; Prazeres, A. R.; Rivas, J. Cheese Whey Wastewater: Characterization and Treatment. *Sci. Total Environ.* **2013**, 445–446, 385–396.
- (4) Nishanthi, M.; Vasiljevic, T.; Chandrapala, J. Properties of Whey Proteins Obtained from Different Whey Streams. *Int. Dairy J.* **2017**, *66*, 76–83.
- (5) Chandrapala, J.; Duke, M. C.; Gray, S. R.; Zisu, B.; Weeks, M.; Palmer, M.; Vasiljevic, T. Properties of Acid Whey as a Function of PH and Temperature. *J. Dairy Sci.* **2015**, *98*, 4352–4363.
- (6) Lievore, P.; Simões, D. R. S.; Silva, K. M.; Drunkler, N. L.; Barana, A. C.; Nogueira, A.; Demiate, I. M. Chemical Characterisation and Application of Acid Whey in Fermented Milk. *J. Food Sci. Technol.* **2015**, 52, 2083–2092.
- (7) USDA. Dairy Products June 2020 Highlights; 2020.
- (8) Ketterings, Q.; Czymmek, K.; Gami, S.; Godwin, G.; Ganoe, K. Guidelines for Land Application of Acid Whey; 2017.
- (9) Menchik, P.; Zuber, T.; Zuber, A.; Moraru, C. I. Short Communication: Composition of Coproduct Streams from Dairy Processing: Acid Whey and Milk Permeate. *J. Dairy Sci.* **2019**, *102*, 3978–3984.
- (10) Peterson, A. A.; Vogel, F.; Lachance, R. P.; Fröling, M.; Antal, M. J., Jr.; Tester, J. W. Thermochemical Biofuel Production in Hydrothermal Media: A Review of Sub- and Supercritical Water Technologies. *Energy Environ. Sci.* **2008**, *1*, 32–65.
- (11) Gami, S.; Godwin, G.; Czymmek, K.; Ganoe, K.; Ketterings, Q. Acid Whey PH and Nutrient Content; 2016.
- (12) Song, W.; Wang, S.; Guo, Y.; Xu, D. Bio-Oil Production from Hydrothermal Liquefaction of Waste Cyanophyta Biomass: Influence of Process Variables and Their Interactions on the Product Distributions. *Int. J. Hydrogen Energy* **2017**, *42*, 20361–20374.
- (13) Gai, C.; Zhang, Y.; Chen, W. T.; Zhang, P.; Dong, Y. Energy and Nutrient Recovery Efficiencies in Biocrude Oil Produced via Hydrothermal Liquefaction of Chlorella Pyrenoidosa. *RSC Adv.* **2014**, *4*, 16958–16967.
- (14) Ekpo, U.; Ross, A. B.; Camargo-Valero, M. A.; Fletcher, L. A. Influence of PH on Hydrothermal Treatment of Swine Manure: Impact on Extraction of Nitrogen and Phosphorus in Process Water. *Bioresour. Technol.* **2016**, *214*, 637–644.
- (15) Ekpo, U.; Ross, A. B.; Camargo-Valero, M. A.; Williams, P. T. A Comparison of Product Yields and Inorganic Content in Process Streams Following Thermal Hydrolysis and Hydrothermal Processing of Microalgae, Manure and Digestate. *Bioresour. Technol.* **2016**, 200, 951–960.
- (16) Ghanim, B. M.; Kwapinski, W.; Leahy, J. J. Speciation of Nutrients in Hydrochar Produced from Hydrothermal Carbonization of Poultry Litter under Different Treatment Conditions. ACS Sustainable Chem. Eng. 2018, 6, 11265–11272.

- (17) Ovsyannikova, E.; Kruse, A.; Becker, G. C. Feedstock-Dependent Phosphate Recovery in a Pilot-Scale Hydrothermal Liquefaction Bio-Crude Production. *Energies* **2020**, *13*, 1379.
- (18) Fan, Y.; Hornung, U.; Dahmen, N.; Kruse, A. Hydrothermal Liquefaction of Protein-Containing Biomass: Study of Model Compounds for Maillard Reactions. *Biomass Conv. Bioref.* **2018**, *8*, 909–923.
- (19) Yang, J.; He, Q. (. S.).; Corscadden, K.; Niu, H.; Lin, J.; Astatkie, T. Advanced Models for the Prediction of Product Yield in Hydrothermal Liquefaction via a Mixture Design of Biomass Model Components Coupled with Process Variables. *Appl. Energy* **2019**, 233-234, 906–915.
- (20) Posmanik, R.; Martinez, C. M.; Cantero-Tubilla, B.; Cantero, D. A.; Sills, D. L.; Cocero, M. J.; Tester, J. W. Acid and Alkali Catalyzed Hydrothermal Liquefaction of Dairy Manure Digestate and Food Waste. ACS Sustainable Chem. Eng. 2018, 6, 2724–2732.
- (21) R., Singh; Krishna, B. B.; Bhaskar, T. Hydrothermal Liquefaction of Lignocellulosic Biomass Components: Effect of Alkaline Catalyst. In *Biofuels*; Agarwal, A., Agarwal, R., Gupta, T., Gurjar, B., Eds.; Springer: Singapore, 2017. DOI: 10.1007/978-981-10-3791-7.
- (22) Zhang, B.; He, Z.; Chen, H.; Kandasamy, S.; Xu, Z.; Hu, X.; Guo, H. Effect of Acidic, Neutral and Alkaline Conditions on Product Distribution and Biocrude Oil Chemistry from Hydrothermal Liquefaction of Microalgae. *Bioresour. Technol.* **2018**, 270, 129–137.
- (23) Makut, B. B.; Goswami, G.; Das, D. Evaluation of Bio-Crude Oil through Hydrothermal Liquefaction of Microalgae-Bacteria Consortium Grown in Open Pond Using Wastewater. *Biomass Conv. Bioref.* **2020**, 1–15.
- (24) Madsen, R. B.; Glasius, M. How Do Hydrothermal Liquefaction Conditions and Feedstock Type Influence Product Distribution and Elemental Composition? *Ind. Eng. Chem. Res.* **2019**, *58*, 17583–17600.
- (25) Yang, C. M.; Lee, C. G.; Won, J. I. Improvement of Bio-Crude Oil Yield and Phosphorus Content by Hydrothermal Liquefaction Using Microalgae. *Chem. Eng. Technol.* **2017**, *40*, 2188–2196.
- (26) Posmanik, R.; Labatut, R. A.; Kim, A. H.; Usack, J. G.; Tester, J. W.; Angenent, L. T. Coupling Hydrothermal Liquefaction and Anaerobic Digestion for Energy Valorization from Model Biomass Feedstocks. *Bioresour. Technol.* **2017**, 233, 134–143.
- (27) Wang, Y.; Xiao, Y.; Xiao, G. Sustainable Value-Added C 3 Chemicals from Glycerol Transformations: A Mini Review for Heterogeneous Catalytic Processes. *Chin. J. Chem. Eng.* **2019**, 27, 1536–1542.
- (28) Liu, H.; Chen, Y.; Yang, H.; Gentili, F. G.; Söderlind, U.; Wang, X.; Zhang, W.; Chen, H. Conversion of High-Ash Microalgae through Hydrothermal Liquefaction. *Sustain. Energy Fuels* **2020**, *4*, 2782–2791.
- (29) Costa, N. R.; Lourenço, J.; Pereira, Z. L. Desirability Function Approach: A Review and Performance Evaluation in Adverse Conditions. *Chemom. Intell. Lab. Syst.* **2011**, *107*, 234–244.
- (30) Amdoun, R.; Khelifi, L.; Khelifi-Slaoui, M.; Amroune, S.; Asch, M.; Assaf-ducrocq, C.; Gontier, E. The Desirability Optimization Methodology; a Tool to Predict Two Antagonist Responses in Biotechnological Systems: Case of Biomass Growth and Hyoscyamine Content in Elicited Datura Starmonium Hairy Roots. *Iran. J. Biotechnol.* **2018**, *16*, 11–19.
- (31) NIST/SEMATECH. E-Handbook of Statistical Methods; National Institute of Standards and Technology, 2013. .
- (32) Gorissen, S. H. M.; Crombag, J. J. R.; Senden, J. M. G.; Waterval, W. A. H.; Bierau, J.; Verdijk, L. B.; van Loon, L. J. C. Protein Content and Amino Acid Composition of Commercially Available Plant-Based Protein Isolates. *Amino Acids* **2018**, *50*, 1685–1695.
- (33) Liu, J.; Klebach, M.; Visser, M.; Hofman, Z. Amino Acid Availability of a Dairy and Vegetable Protein Blend Compared to Single Casein, Whey, Soy, and Pea Proteins: A Double-Blind, Cross-Over Trial. *Nutrients* **2019**, *11*, 2613.
- (34) Obeid, R.; Lewis, D. M.; Smith, N.; Hall, T.; Van Eyk, P. Reaction Kinetics and Characterization of Species in Renewable Crude from Hydrothermal Liquefaction of Mixtures of Polymer Compounds to Represent Organic Fractions of Biomass Feedstocks. *Energy Fuels* **2020**, 34, 419–429.

- (35) Posmanik, R.; Cantero, D. A.; Malkani, A.; Sills, D. L.; Tester, J. W. Biomass Conversion to Bio-Oil Using Sub-Critical Water: Study of Model Compounds for Food Processing Waste. *J. Supercrit. Fluids* **2017**, *119*, 26–35.
- (36) Wang, K.; Ma, Q.; Burns, M.; Sudibyo, H.; Sills, D. L.; Goldfarb, J. L.; Tester, J. W. Impact of Feed Injection and Batch Processing Methods in Hydrothermal Liquefaction. *J. Supercrit. Fluids* **2020**, *164*, No. 104887.
- (37) Lu, J.; Li, H.; Zhang, Y.; Liu, Z. Nitrogen Migration and Transformation during Hydrothermal Liquefaction of Livestock Manures. ACS Sustainable Chem. Eng. 2018, 6, 13570–13578.
- (38) ASTM. Standard Test Method for Ash in Biomass. ASTM E1755-01, 2008; 545-545-3.
- (39) Hanna Instruments. HI83399 Multiparameter Photometer with COD, https://cdn2.hubspot.net/hubfs/2134380/product-manuals/MAN83399 05 19.pdf.
- (40) American Society for Testing and Materials (ASTM) ASTM D1426-15 Standard Test Methods for Ammonia Nitrogen In Water. 2015, 1–9.
- (41) American Public Health Association (APHA). Standard Methods for the Examination of Water and Wastewater, 20th ed.; Clesceri, L., Greenberg, A., Eaton, A., Eds.; American Public Health Association (APHA): Washington D.C., 1999.
- (42) Crane, K. S.; Webb, B. L.; Allen, P. S.; Jolley, V. D. A Rapid Turbidimetric Potassium Test Modified for Use with the Pressurized Hot-Water Extraction. *Commun. Soil Sci. Plant Anal.* **2005**, *36*, 2687–2697.
- (43) Wells, R. W. Determination of Serum Calcium by Turbidimetry. *Am. J. Clin. Pathol.* **1948**, *18*, 576–578.
- (44) Channiwala, S. A.; Parikh, P. P. A Unified Correlation for Estimating HHV of Solid, Liquid and Gaseous Fuels. *Fuel* **2002**, *81*, 1051–1063.
- (45) Obeid, R.; Lewis, D.; Smith, N.; van Eyk, P. The Elucidation of Reaction Kinetics for Hydrothermal Liquefaction of Model Macromolecules. *Chem. Eng. J.* **2019**, *370*, 637–645.
- (46) Qiu, Y.; Aierzhati, A.; Cheng, J.; Guo, H.; Yang, W.; Zhang, Y. Biocrude Oil Production through the Maillard Reaction between Leucine and Glucose during Hydrothermal Liquefaction. *Energy Fuels* **2019**, 33, 8758–8765.
- (47) Zhang, X.; Li, X.; Li, R.; Wu, Y. Hydrothermal Carbonization and Liquefaction of Sludge for Harmless and Resource Purposes: A Review. *Energy Fuels* **2020**, *34*, 13268–13290.
- (48) Shi, N.; Liu, Q.; He, X.; Wang, G.; Chen, N.; Peng, J.; Ma, L. Molecular Structure and Formation Mechanism of Hydrochar from Hydrothermal Carbonization of Carbohydrates. *Energy Fuels* **2019**, 33, 9904–9915.
- (49) Kruse, A.; Krupka, A.; Schwarzkopf, V.; Gamard, C.; Henningsen, T. Influence of Proteins on the Hydrothermal Gasification and Liquefaction of Biomass. 1. Comparison of Different Feedstocks. *Ind. Eng. Chem. Res.* **2005**, *44*, 3013–3020.
- (50) Singh, R.; Bhaskar, T.; Balagurumurthy, B. Hydrothermal Upgradation of Algae into Value-Added Hydrocarbons. In *Biofuels from Algae*; Pandey, A., Lee, D.-J., Chisti, Y., Soccol, C. R., Eds.; Elsevier, 2014; 235- 260. DOI: 10.1016/B978-0-444-59558-4.00011-5.
- (51) Chen, W. T.; Qian, W.; Zhang, Y.; Mazur, Z.; Kuo, C. T.; Scheppe, K.; Schideman, L. C.; Sharma, B. K. Effect of Ash on Hydrothermal Liquefaction of High-Ash Content Algal Biomass. *Algal Res.* **2017**, *25*, 297–306.
- (52) Minowa, T.; Zhen, F.; Ogi, T. Cellulose Decomposition in Hot-Compressed Water with Alkali or Nickel Catalyst. *J. Supercrit. Fluids* **1998**, *13*, 253–259.
- (53) Vardon, D. R.; Sharma, B. K.; Scott, J.; Yu, G.; Wang, Z.; Schideman, L.; Zhang, Y.; Strathmann, T. J. Chemical Properties of Biocrude Oil from the Hydrothermal Liquefaction of Spirulina Algae, Swine Manure, and Digested Anaerobic Sludge. *Bioresour. Technol.* **2011**, *102*, 8295–8303.
- (54) Gollakota, A. R. K.; Kishoreb, N.; Gua, S. A Review on Hydrothermal Co-Liquefaction of Biomass. *Renew. Sustain. Energy Rev.* **2018**, *81*, 1378–1392.

- (55) Chen, J.; Li, S. Characterization of Biofuel Production from Hydrothermal Treatment of Hyperaccumulator Waste (Pteris Vittata L.) in Sub-And Supercritical Water. *RSC Adv.* **2020**, *10*, 2160–2169.
- (56) Bayat, H.; Dehghanizadeh, M.; Jarvis, J. M.; Brewer, C. E.; Jena, U. Hydrothermal Liquefaction of Food Waste: Effect of Process Parameters on Product Yields and Chemistry. *Front. Sustain. Food Syst.* **2021**, *5*, 1–16.
- (57) Qian, L.; Wang, S.; Savage, P. E. Fast and Isothermal Hydrothermal Liquefaction of Sludge at Different Severities: Reaction Products, Pathways, and Kinetics. *Appl. Energy* **2020**, *260*, No. 114312.
- (58) Sharma, K.; Shah, A. A.; Toor, S. S.; Seehar, T. H.; Pedersen, T. H.; Rosendahl, L. A. Co-Hydrothermal Liquefaction of Lignocellulosic Biomass in Supercritical Water. *Energies* **2021**, *14*, 1708.
- (59) Fan, Y.; Hornung, U.; Raffelt, K.; Dahmen, N. The Influence of Lipids on the Fate of Nitrogen during Hydrothermal Liquefaction of Protein-Containing Biomass. J. Anal. Appl. Pyrolysis 2020, 147, No. 104798.
- (60) Jazrawi, C.; Biller, P.; He, Y.; Montoya, A.; Ross, A. B.; Maschmeyer, T.; Haynes, B. S. Two-Stage Hydrothermal Liquefaction of a High-Protein Microalga. *Algal Res.* **2015**, *8*, 15–22.
- (61) Peterson, A. A.; Lachance, R. P.; Tester, J. W. Kinetic Evidence of the Maillard Reaction in Hydrothermal Biomass Processing: Glucose-Glycine Interactions in High-Temperature, High-Pressure Water. *Ind. Eng. Chem. Res.* **2010**, *49*, 2107–2117.
- (62) Guan, Y. G.; Wang, S. L.; Yu, S. J.; Yu, S. M.; Zhao, Z. G. Changes in the Initial Stages of a Glucose-Proline Maillard Reaction Model System Influences Dairy Product Quality during Thermal Processing. *J. Dairy Sci.* **2012**, *95*, 590–601.
- (63) Robinson, K. J.; Gould, I. R.; Fecteau, K. M.; Hartnett, H. E.; Williams, L. B.; Shock, E. L. Deamination Reaction Mechanisms of Protonated Amines under Hydrothermal Conditions. *Geochim. Cosmochim. Acta* **2019**, 244, 113–128.
- (64) Prado, G. H. C.; Rao, Y.; De Klerk, A. Nitrogen Removal from Oil: A Review. *Energy Fuels* **2017**, *31*, 14–36.
- (65) Voisin, T.; Erriguible, A.; Ballenghien, D.; Mateos, D.; Kunegel, A.; Cansell, F.; Aymonier, C. Solubility of Inorganic Salts in Sub- and Supercritical Hydrothermal Environment: Application to SCWO Processes. *J. Supercrit. Fluids* **2017**, *120*, 18–31.